Materials and Design 51 (2013) 665–675

Contents lists available at SciVerse ScienceDirect

Materials and Design

journal homepage: www.elsevier.com/locate/matdes

Microstructure and fatigue properties of fiber laser welded dissimilar joints between high strength low alloy and dual-phase steels

D. Parkes [a], W. Xu [a], D. Westerbaan [b], S.S. Nayak [b], Y. Zhou [b], F. Goodwin [c], S. Bhole [a], D.L. Chen [a,*]

[a] Department of Mechanical and Industrial Engineering, Ryerson University, 350 Victoria Street, Toronto, ON M5B 2K3, Canada
[b] Department of Mechanical and Mechatronics Engineering, University of Waterloo, 200 University Avenue West, Waterloo, ON N2L 3G1, Canada
[c] International Zinc Association, Durham, NC 27713, USA

ARTICLE INFO

Article history:
Received 9 March 2013
Accepted 20 April 2013
Available online 30 April 2013

Keywords:
Fiber laser welding
Dissimilar joint
High strength low alloy steel
Dual-phase steel
Microstructure
Fatigue

ABSTRACT

The aim of this study was to evaluation the microstructure and fatigue properties of welded joints made with fiber laser welding (FLW) on a high strength low alloy (HSLA) and dual-phase (DP980, UTS $\geqslant$ 980 MPa) steel in similar and dissimilar material combinations. The fusion zone (FZ) consisted of martensite, and the heat affected zone (HAZ) contained some newly formed martensite and partially tempered martensite on the DP980 steel side. A characteristic asymmetric hardness profile across the dissimilar HSLA–DP980 welded joint was observed. While a soft zone occurred on the DP980 side, it was absent on the HSLA side. Inside the FZ two hardness sub-regions were observed due to the difference in the alloying elements between two steels along with the fast cooling during FLW. The presence of soft zone on the DP980 side had no effect on the tensile properties, since the lowest hardness value in the soft zone was still higher than that of the HSLA base metal (BM). A joint efficiency of 97–100% was achieved with respect to the HSLA. The strain to failure of the dissimilar HSLA–DP980 welded joints was significantly (~threefold) higher than that of the similar DP980–DP980 welded joints. Although the fatigue strength of the dissimilar HSLA–DP980 welded joints was lower than that of DP980–DP980 welded joints, it was equivalent to that of HSLA–HSLA welded joints. Failure occurred in the BM on the HSLA side in the tensile tests and fatigue tests at high cyclic stress levels, where yielding occurred. At the intermediate and lower cyclic stress levels, fatigue failure occurred in the weld area due to the higher sensitivity to the weld concavity.

© 2013 Elsevier Ltd. All rights reserved.

1. Introduction

In the highly competitive automotive market along with the vast energy and environment concerns [1,2], the car manufacturers are constantly looking for better materials and products to add to their line-up of vehicles in order to get an edge on their competitors, and especially reduce fuel consumption and CO_2 emissions. This can be achieved via an effective weight reduction of motor vehicles [2,3] using stronger and thinner sheet materials, without compromising ductility and formability, to replace the conventional and lower strength automotive materials [4–9]. This idea has led to the development of a family of advanced high strength steel (AHSS), which is being increasingly implemented for automotive body-in-white applications due to the excellent combination of high strength with good formability [4,5]. Dual-phase (DP) steel is one of the popular members in the AHSS family [6,10,11], which is produced through inter-critical annealing followed by quenching to form a two-phase microstructure containing martensite islands embedded in the ferrite matrix. On the other hand, high strength low alloy (HSLA) steel is a more commonly used automotive steel which consists of fine ferrite grains with dispersed ultra-fine alloy carbides [7,10,12,13]. Currently, several grades of DP steel are being considered to replace, partly but not completely, HSLA steel in manufacturing auto-body components where higher strength is necessary, e.g., B-pillars and bumpers [8,14].

The primary manufacturing process used in auto-body fabrication is welding, it is thus important to understand the metallurgical and mechanical phenomena involved in the welding of DP, HSLA steels and especially their dissimilar combination. Furthermore, laser welding is usually used to manufacture welded blanks which are formed into different shapes of the auto-body parts [13,15–20]. Fiber laser, diode laser, Nd:YAG laser, and CO_2 laser are the primary types of laser welding techniques available which have been previously applied to weld a variety of steels to evaluate and compare their benefits and detriments [15–19,21]. Amongst these laser welding processes, fiber laser welding (FLW) is the newest one with several advantages over other types, including

* Corresponding author. Tel.: +1 416 979 5000x6487; fax: +1 416 979 5265.
E-mail address: dchen@ryerson.ca (D.L. Chen).

0261-3069/$ - see front matter © 2013 Elsevier Ltd. All rights reserved.
http://dx.doi.org/10.1016/j.matdes.2013.04.076

smaller beam divergence, low maintenance costs, higher efficiency, high precision and reliability, and compact size [13,20,22,23]. Thus, superior quality welds are able to be generally produced in FLW.

There were a number of studies on the laser welding of DP980 and HSLA welded joints [13,15–19]. An important phenomenon that has commonly been observed in the DP980 welds is the formation of a "soft zone" at the outer HAZ (also termed as HAZ softening), i.e., a drop in hardness below that of the BM [13,15–19]. The HAZ softening was observed to be dependent on the grade of the DP steel and the type of laser welding process. The degree of HAZ softening also has a strong influence on the performance, e.g., formability, tensile properties, and fatigue resistance of the welded joints [13,15–19,24]. After comparing several types of lasers, it was concluded that the FLW is more beneficial in minimizing the HAZ softening, in both the magnitude of softening and the width of soft zone, due to the higher power density as a result of the narrower beam diameter, which allows welding at higher speeds.

To facilitate the design of laser welded blanks and promote a widespread use of DP steels in the automotive industry, the relationships between the microstructural change involved in FLW and the static and dynamic performance of the welded joints must be evaluated so as to guarantee the reliability and durability of the parts as well as the overall safety of the passenger vehicles. In this regard the authors [13] have recently reported a study on the mechanical behavior of FLW DP980 and HSLA steels in similar combinations. No studies have been reported so far on the dissimilar combination of DP980 and HSLA using the FLW process. The present study is an extension of the previous work, which was aimed at characterizing the dissimilar fiber laser welded joints of DP980 and HSLA with respect to the microstructure change and fatigue performance.

2. Experimental details

The starting materials in this study were HSLA and DP980 (UTS $\geqslant$ 980 MPa) steel sheets (1.2 mm thick) with galvanized (GI) coating. The chemical compositions of the steels are listed in Table 1. Welded blanks with a dimension of 200 mm $\times$ 200 mm were fabricated by laser butt welding 100 mm $\times$ 200 mm sheets in an IPG Photonics YLS-6000 fiber laser system attached to a Panasonic robotic arm. A laser power of 6 kW, with a beam focal length of 20 cm, a spot size of 0.6 mm, and a welding speed of 16 m/min were used to weld the blanks. The fiber laser had a fiber core diameter of 0.3 mm with a laser beam spot size/diameter of 0.6 mm. Welding was performed with a head angle of 0°, i.e., the laser beam was perpendicular to the steel sheets being welded. No shielding gas was used during the welding process. A schematic illustration of the welded blank is shown in Fig. 1a. It should be noted that a little concavity was observed in all the welds, and the subsequent mechanical testing was carried on the samples in the as-welded state without any post-weld processing.

The metallographic samples used for the examination of microstructural changes were cut from the weld cross-section, then mounted, ground, polished, and etched with a 2% Nital solution. The etched samples were observed first using a light microscope attached with Clemex image analysis system software and then with a scanning electron microscope (JEOL JSM-6380) equipped with Oxford energy dispersive X-ray spectroscopy (EDS) and three-dimensional fractographic analysis capacity. Vickers microhardness was measured on the polished samples across the weld using a computerized microhardness tester using a load of 200 g and a dwell time of 15 s. All indentations were adequately spaced to prevent any potential effect of localized strain hardening caused by adjacent indentations. To ensure the validity of each test result, two calibration tests were carried out using a standard reference test block before the microhardness tests on the welded joints were conducted.

Tensile and fatigue test samples were machined from the welded blanks perpendicular to the welding direction in accordance with ASTM: E8/E8M, the example of which is indicated by the dashed line in Fig. 1a with the geometry and dimensions of the test coupons shown in Fig. 1b. The specimens were machined in such a way that the weld line was positioned at the center of the gauge length (Fig. 1b). Tensile tests were conducted using a fully computerized United tensile testing machine at room temperature at a strain rate of $1 \times 10^{-3}\ s^{-1}$. An extensometer with a gauge length of 50 mm and a strain limit of 20% was used to measure the strain during the tensile tests. Load control fatigue tests in line with ASTM: E466 were performed on a fully computerized Instron 8801 servo-hydraulic testing system. To avoid potential buckling of the test specimens, tension–tension cyclic loading at a stress ratio of $R = 0.1$ was applied at a frequency of 50 Hz and sinusoidal waveform. At least two specimens were tested in the tensile tests and fatigue tests at each of the cyclic stress amplitude. After the fatigue tests were completed, the fatigue fracture surfaces were examined via scanning electron microscopy (SEM) to identify the fatigue crack initiation sites and the propagation mechanism.

Table 1
Chemical composition of the HSLA and DP980 steel investigated.

Steel grade	C	Mn	Si	Al	Ni	Cr	N	Fe
HSLA	0.08	0.80	0.46	0.05	0.01	0.03	0.007	Balance
DP980	0.15	1.45	0.33	0.05	0.01	0.02	0.009	Balance

3. Results and discussion

3.1. Microstructure evolution

The microstructure of the HSLA–HSLA and DP980–DP980 welded joints are shown in Fig. 2. A significant change in microstructure can be seen across the welded joints, i.e., the formation of fusion zone (FZ) and HAZ which co-existed with the unaffected BM at both sides of the weld as indicated in Fig. 2a and e. The HSLA BM microstructure consisted of fine grained ferrite matrix with a uniform dispersion of fine alloy carbides (Fig. 2b). Fig. 2c shows the microstructure in the HAZ of the HSLA welded joints, which was taken from the position marked by "c" in Fig. 2a. The details of HAZ microstructure will be discussed later in the section. The FZ microstructure (Fig. 2d) contained basically martensitic structure with a lathy morphology. The microstructure developed in the FZ was strongly dependent on the cooling rate involved in the welding process. The continuous-cooling transformation (CCT) diagram of weld metal of low carbon steel shows that the FZ microstructure, depending on the cooling rate, could contain a combination of grain boundary ferrite, side-plate ferrite, acicular ferrite, bainite, and/or martensite [13,25,26]. Thus, the martensite structure formed in the FZ of HSLA in this study was attributed to the high cooling rate during the FLW process, stemming from the high welding speed (16 m/min). The DP980 BM consisted of martensite phase (grey area) embedded in a continuous ferrite (bright area) matrix (Fig. 2f). Fig. 2g shows the microstructural changes occurred within the HAZ of the DP980 welded joint, which was taken from the position marked as "g" in Fig. 2e, the details of which will be discussed later. The microstructure of the FZ in Fig. 2h clearly shows a highly martensitic structure which was attributed to the high cooling rate involved in the FLW and also to the higher hardenability of DP980 steel as a result of the higher content of manganese and carbon (Table 1) [25,26].

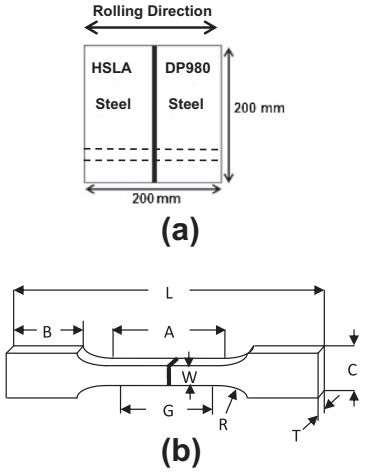

Name	G	W	R	L	A	B	C	T
Dimension (mm)	50	12.5	12.5	200	57	50	20	1.2

Fig. 1. Schematic illustrations of the (a) laser welded blank and (b) tensile and fatigue test specimen machined from and parallel to the region marked by the short-dashed lines in (a).

The microstructural changes of a typical dissimilar HSLA–DP980 welded joint are shown in Fig. 3. The dissimilar welded joint exhibited distinct HAZ on each side of the weld due to the difference in the BM microstructures between DP980 (Fig. 3b) and HSLA (Fig. 3f), which transformed differently when subjected to the FLW thermal cycle. Fig. 3c shows the HAZ on the DP980 side of the welded joint which contained similar microstructural constituents observed in the HAZ of DP980 welded joint (Fig. 2g). Similarly, the HSLA HAZ (Fig. 3e) also resembled closely to the HAZ microstructure obtained in the HSLA welded joint (Fig. 2)c. The micrograph taken from the center of the FZ in the dissimilar welded joints (Fig. 3d) indicated the formation of martensitic structure as well, with the morphology similar to that in the FZ observed in the DP980 welded joint (Fig. 2h), suggesting an insignificant effect of chemical dilution on the FZ microstructure which needs to be analyzed in detail for further understanding. Furthermore, it is seen from Figs. 2 and 3 that the width of the HAZ and FZ in all the welded joints (i.e., HSLA, DP980, and dissimilar) was similar and measured to be in the range of 200–300 μm and 400–500 μm [13].

Fig. 4 shows the SEM images detailing the HAZ microstructure obtained in DP980 welded joint. The DP980 HAZ contained three different regions (Fig. 4a), namely tempered HAZ that experienced temperature below Ac_1 line, intercritical HAZ which is the region of temperatures between Ac_1 and Ac_3 lines, and upper-critical HAZ encountering temperatures above Ac_3 line. The BM microstructure of the DP980 steel (Fig. 4b) corresponded to the optical image shown in 3b). The volume fraction of martensite in the DP980 BM was estimated to be ~56% using image analysis attached to the SEM. The tempered HAZ sub-critical area showed some of the pre-existing martensite from the BM decomposed into partially tempered martensite (PTM), as can be clearly seen in Fig. 4c. Tempering of BM martensite in the fusion welding of DP980 steel has been reported in several previous studies [13,15–19,24]. In the intercritical HAZ (Fig. 4d) austenite started to form since the temperature rose above Ac_1 line of the steel which subsequently transformed to form martensite which was different from BM martensite and the volume fraction of which increased as we moved away from the Ac_1 line (tempered and intercritical HAZ boundary) towards the Ac_3 line (boundary between intercritical and upper-critical HAZ) as can be seen in Fig. 4a. The upper-critical HAZ showed an increased fraction of transformed martensite as compared to the inter-critical HAZ (Fig. 4e).

The SEM image showing the inter-critical and the upper-critical regions of the HAZ in the HSLA welded joint is presented in Fig. 5a. The HSLA BM microstructure (Fig. 5b) was confirmed to consist of ferrite grains with finely dispersed alloy carbide particles. It should be noted here that unlike DP980, HSLA steel was not expected to undergo any phase transformation below A_{c1} line, so that the tempered HAZ was not observed in the welded joint. Fig. 5c presents the inter-critical HAZ microstructure containing ferrite, martensite and bainite which formed as solid state transformation products of austenite. In the upper-critical HAZ (Fig. 5d), more martensite formed, along with a smaller amount of ferrite and bainite.

3.2. Hardness profile

The microhardness profile across the dissimilar HSLA–DP980 welded joint is presented in Fig. 6. It is seen that the hardness profile exhibited an asymmetric characteristic with a higher hardness on the DP980 side and a lower hardness on the HSLA side. In particular, a soft zone appeared on the DP980 side, but it was absent on the HSLA side. For the sake of a better comparison, the hardness data across the similar HSLA–HSLA and DP980–DP980 welded joints are plotted in Fig. 7. It is seen that both the HSLA–HSLA welded joint and the HSLA side of the dissimilar HSLA–DP980 welded joint had a similar trend of hardness variation with a constant and uniform BM hardness followed by a sharp increase through the HAZ up into the FZ. This was due to the fact that the microstructure of the HSLA BM was composed of fine ferrite grains with dispersed alloy carbides (Fig. 5b), while in the intercritical and upper-critical zones of the HAZ, there was a gradual transformation into martensite which accounted for the increase in hardness up to the FZ with a highly martensitic structure (Fig. 5) [13]. It is also seen from Fig. 7 that the hardness change on the DP980 side of the dissimilar welded joint was equivalent to that of similar DP980–DP980 welded joint, where there was a relatively high hardness in the BM arising from the structure of a ferrite matrix with a higher volume faction of martensite (Figs. 3b and 4b). From the BM across the HAZ into the FZ, a soft zone in the HAZ formed in the sub-critical region, where the temperature experienced in the

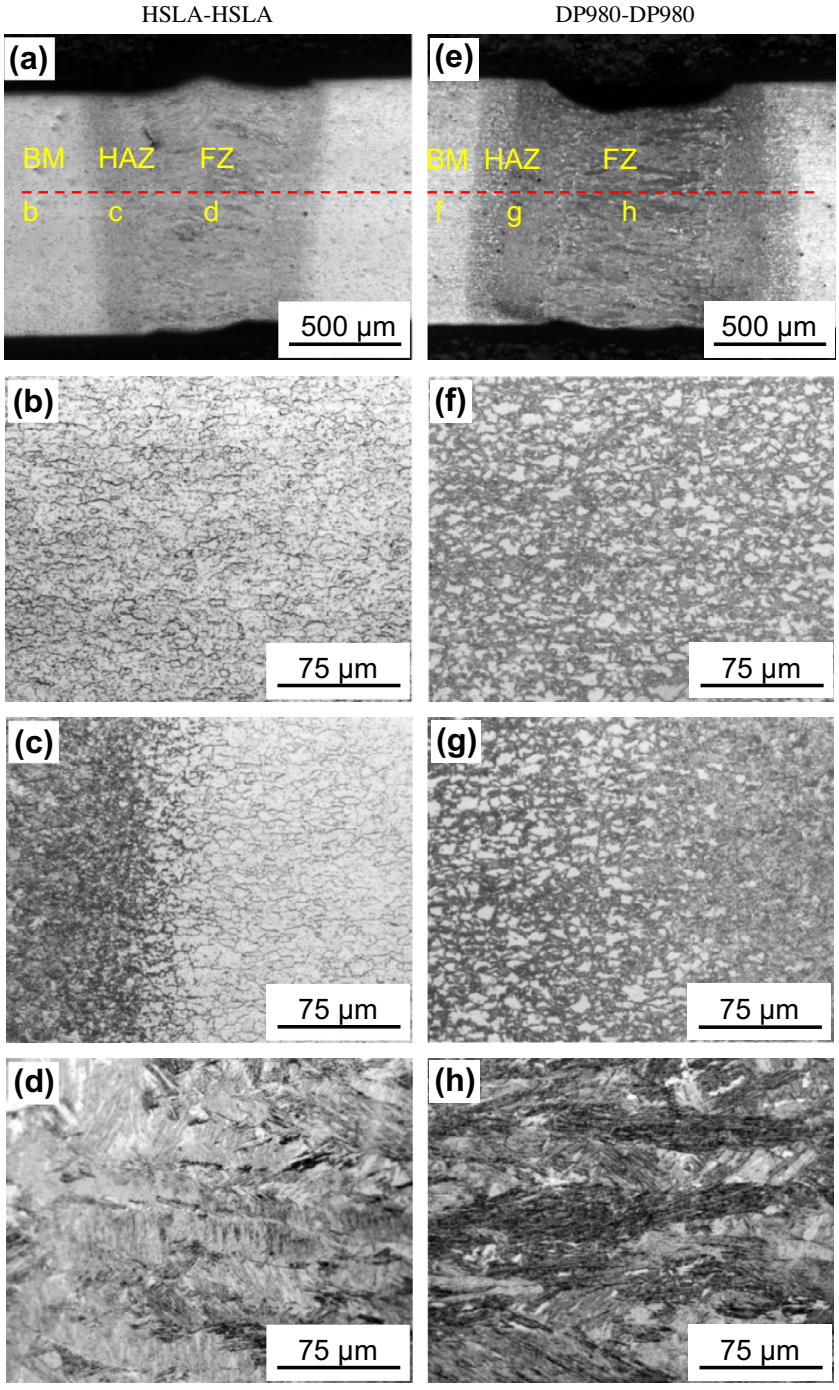

Fig. 2. Light microscopy images showing the microstructure in the welded joints of HSLA ((a): overall view, (b): BM, (c): HAZ and (d): FZ) and DP980 ((e): overall view, (f): BM, (g): HAZ and (h): FZ) steel.

welding process was below the Ac_1 line of the steel, leading to tempering of BM martensite with a extent of tempering decreasing with decreasing temperature, i.e., moving away from the Ac_1 line towards the BM. Martensite is known to have a metastable body-centered tetragonal (BCT) structure, and the high temperatures experienced during FLW would activate the diffusion of carbon and convert the martensite into tempered martensite (ferrite and Fe_3C cementite) with a lower hardness. This tempering effect resulted in a localized decrease in hardness as seen in the hardness profile (Figs. 6 and 7) as a valley [13,15,17,24,27,28].

It is of particular interest to observe that inside the FZ there were two distinct hardness sub-regions associated with two different materials (i.e., ~390HV on the HSLA side and ~410HV on the DP980 side). This was a result of the difference in chemistry between HSLA and DP980, where the carbon and manganese contents of DP980 were higher than that of HSLA (nearly doubled as listed in Table 1), leading to a higher carbon martensite upon solidification and rapid cooling in the vicinity of DP980 steel. That is, the hardenability in the sub-region near the DP980 steel was higher due to the presence of a higher amount of alloying elements [25,26]. Since the time involved in the liquid state and the subsequent solidification during the FLW was very short, there was little or insufficient diffusion in the FZ, which implied that the FZ was still in the form of segregation between the two materials. This is

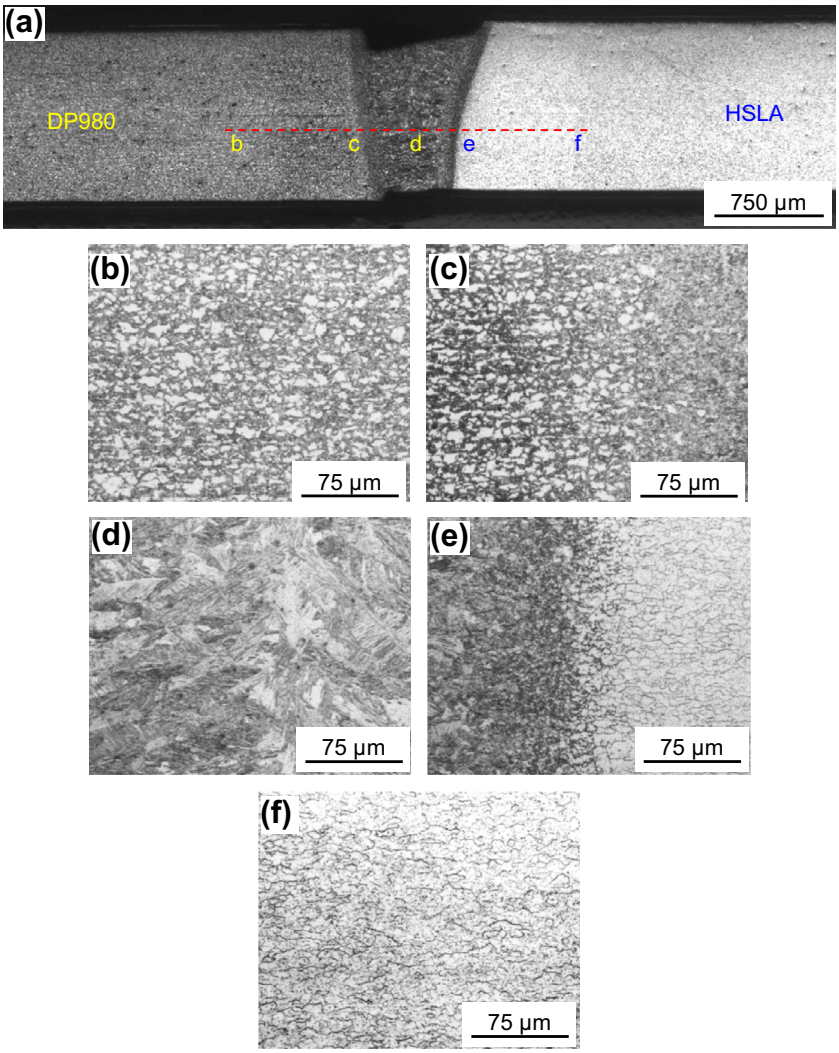

Fig. 3. Micrographs showing the microstructure change of a dissimilar HSLA–DP980 welded joint, (a) overall view, (b) DP980 BM, (c) HAZ on the DP980 steel side, (d) FZ, (e) HAZ on the HSLA steel and (f) HSLA BM.

why two sub-regions could be observed in the FZ of the dissimilar HSLA–DP980 welded joint (Fig. 6), although the morphology and amount of martensite appeared roughly the same (Fig. 2d and h).

3.3. Tensile properties

The representative engineering stress versus engineering strain curves of the similar HSLA–HSLA and DP980–DP980, and dissimilar HSLA–DP980 welded joints are illustrated in Fig. 8. The details of the tensile test results are given in Table 2. In the similar HSLA–HSLA welded joints, the yield strength (YS), ultimate tensile strength (UTS), and the strain to failure after FLW were observed to be very close to those of the BM within the experimental scatter. For example, the YS and UTS of the HSLA–HSLA welded joints were obtained to be 446 MPa and 529 MPa, respectively, which were very close to those of the BM which had a YS of 455 MPa and UTS of 546 MPa, respectively, with a joint efficiency of 97% (Table 2). These tensile results suggested that the FLW process did not deteriorate the tensile properties of the HSLA steel, which was apparently attributed to the fact that in the HSLA–HSLA welded joints no soft zone occurred in the HAZ (Figs. 6 and 7) that was detrimental to the mechanical properties of the welds [13]. This was also corroborated by the observations that the failure of HSLA–HSLA welded joints during tensile testing consistently occurred in the BM.

In contrast to the HSLA–HSLA welded joints, the DP980–DP980 welded joints showed a lower strain to failure (5.3%). However, the UTS (1067 MPa) was also very close to that of the DP980 BM (1095 MPa), indicating a high joint efficiency (97%) as well (Fig. 8 and Table 2). Obviously, the strength of the DP980–DP980 welded joints made with the FLW did not decrease in spite of the presence of soft zone, while the strength of the joints made with the diode laser welding (DLW) exhibited a fair amount of decrease [16,28]. This was obviously related to the narrower and less severe soft zone in the present fiber laser welded joints (Figs. 6 and 7). It follows that the smaller laser beam spot size and higher power intensity in conjunction with a higher welding speed in the FLW greatly improved the strength of the welded joints by reducing the detrimental effects of soft zone by narrowing it down significantly. However, the decrease in ductility of the DP980–DP980 welded joints was still attributed to the presence of soft zone. With progressive loading beyond the UTS, the plastic deformation of the similar DP980–DP980 welded joints concentrated in the soft zone due to its lower strength, causing a premature failure and thus a lower strain to failure [13,28]. Similar results were also reported by Hazratinezhad et al. [24] using a DP980 steel with an Nd:YAG laser.

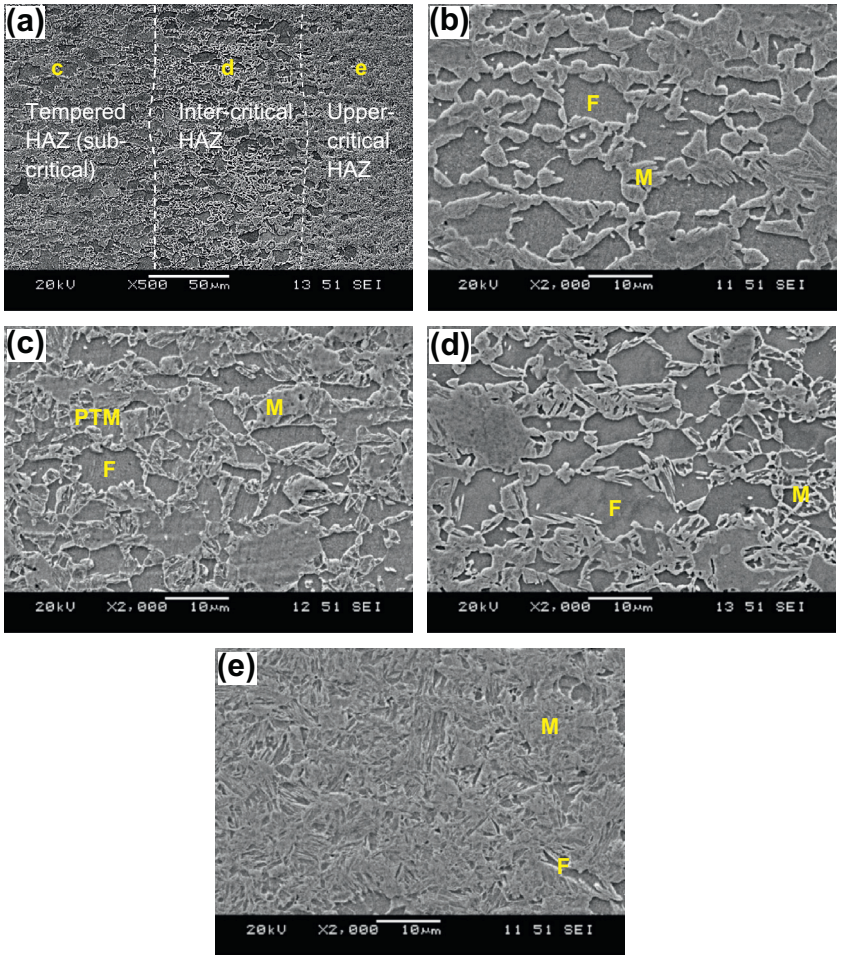

Fig. 4. SEM micrographs showing the microstructure of martensite change in a DP980 welded joint, (a) overall view of the HAZ, (b) DP980 BM showing ferrite and martensite phases, (c) tempered martensite in the sub-critical HAZ, (d) the intercritical region and (e) upper-critical region showing new martensite formed by rapid cooling of austenite (M: martensite, PTM: partially tempered martensite, and F: ferrite).

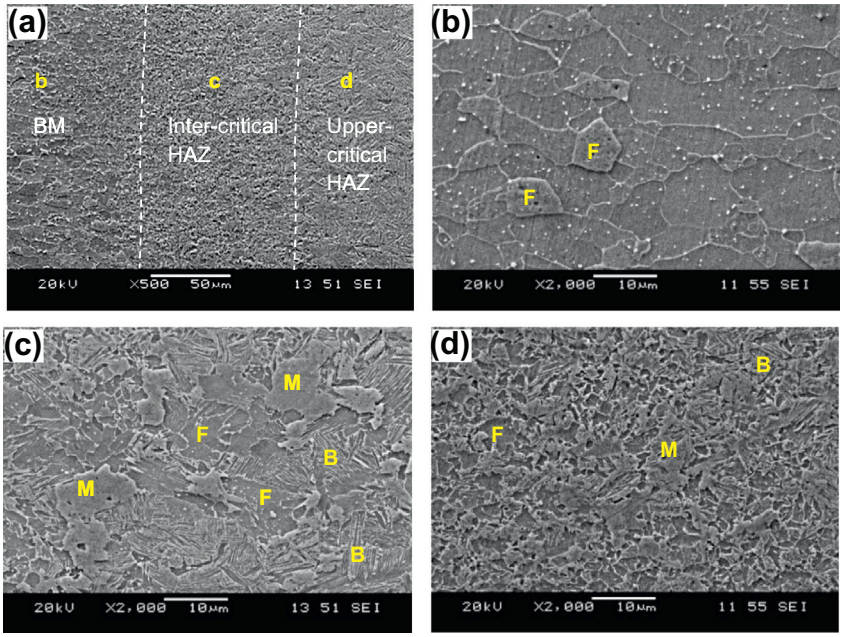

Fig. 5. SEM micrographs showing the microstructure in the HAZ of the HSLA welded joint: (a) overview of the BM, intercritical HAZ, and upper-critical HAZ, (b) BM microstructure delineating fine alloy carbides in a ferrite matrix, and (c) intercritical HAZ showing bainite and new martensite (d) upper-critical HAZ indicated increased fraction of newly form martensite and bainite phases. (M: martensite, B: bainite, and F: ferrite).

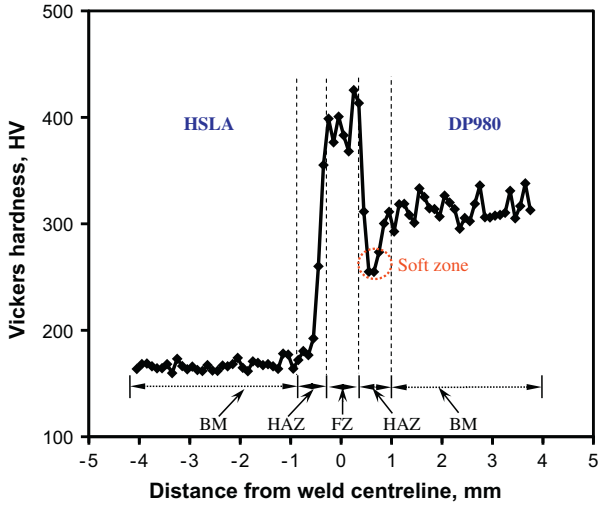

Fig. 6. Microhardness profile across the dissimilar HSLA–DP980 welded joint.

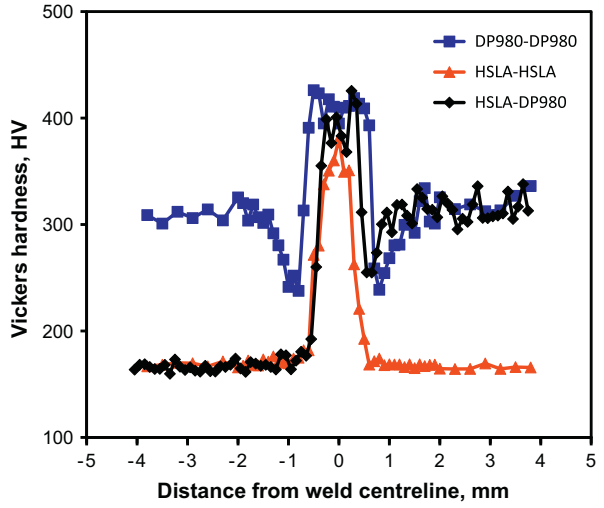

Fig. 7. A comparison of hardness for the HSLA, DP980, and dissimilar welded joints made at a welding speed of 16 m/min, where the hardness data for the HSLA–HSLA and DP980–DP980 similar joints were taken from Ref. [13].

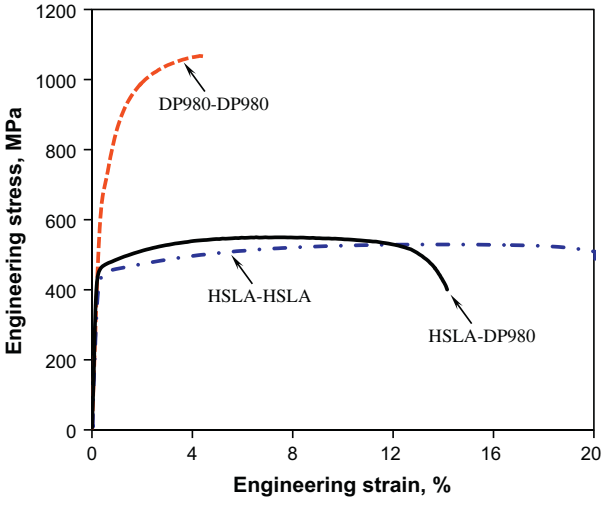

Fig. 8. Representative engineering stress versus engineering strain curves of the HSLA, DP980, and dissimilar welded joints tested at a strain rate of 1×10^{-3} s^{-1}.

As seen from Table 2, while the YS (467 MPa) and UTS (548 MPa) of the dissimilar HSLA–DP980 welded joints were well below those of the similar DP980–DP980 welded joints, they were essentially the same as those of the HSLA BM or similar HSLA–HSLA welded joints. Based on the UTS of HSLA BM rather than that of DP980 BM, the joint efficiency of the present dissimilar HSLA–DP980 welded joints indeed reached about 100%. It should be noted that the experimentally obtained slightly higher YS and UTS of the dissimilar HSLA–DP980 welded joints than those of HSLA BM were considered to be due to the experimental error, since it would be impossible to have a joint efficiency of over 100%. It of special interest to observe that the dissimilar HSLA–DP980 welded joints showed a considerable (nearly threefold) improvement in the strain to failure (15.4%), compared with the similar DP980–DP980 welded joints (5.3%), although it was lower than that of the similar HSLA–HSLA welded joints (22.3%). It was observed that the DP980 side of the dissimilar weld did not yield at all during tensile testing, with almost all the plastic deformation taking place on the HSLA side. Panda et al. [9] reported similar results in a limited dome height formability test of a DLW HSLA–DP980 sheet. It is clear that the presence of the soft zone in the HAZ of the DP980 side did not have any effect on the YS and UTS of the dissimilar HSLA–DP980 welded joints. This was understandable since the lowest hardness value at the valley of soft zone (255HV) was still higher than that of the HSLA BM (167HV), as shown in Fig. 6. As a result, only HSLA would yield during tensile loading.

3.4. Fatigue properties

Fatigue tests of the similar HSLA–HSLA and DP980–DP980, and dissimilar HSLA–DP980 welded joints were carried out at room temperature at a stress ratio of $R = 0.1$, and the obtained S–N curves are plotted in Fig. 9. Like the tensile testing, the dissimilar HSLA–DP980 welded joints behaved nearly the same as the similar HSLA–HSLA welded joints. The similar DP980–DP980 welded joints exhibited a much higher fatigue strength in the low cycle fatigue regime below $\sim 5 \times 10^4$ cycles, although there was no big difference in the high cycle fatigue regime where the experimental scatter also became larger. At a high stress amplitude of 350–450 MPa in the similar DP980–DP980 welded joints, some yielding would occur since the maximum stress at $R = 0.1$ exceeded the YS of 720 MPa (Table 2). As the stress amplitude decreased, the fatigue life became longer but more scattered. This was due to a more sensitive effect of the soft zone in the HAZ and the concavity [29] that was present in the welded joints, as shown in Fig. 2e. Similar weld concavity was reported in [28,30,31] as well.

Likewise, in the similar HSLA–HSLA welded joints and dissimilar HSLA–DP980 welded joints, at high stress amplitudes of 225–250 MPa, the peak stress was above the yield stress of HSLA BM (Table 2), causing the yielding and failure in the BM, as shown in Fig. 10a. At the lower stress amplitudes (i.e., below 200 MPa) there was a larger scatter in the experimental data since the samples failed in the weld area (Fig. 10b and c), which was related to the stress concentration developed by the concavity in the welds [30,31]. Since the samples that are subjected to cyclic loading were reported to be more susceptible to heterogeneous changes in the microstructure than those done in a tensile test [30,32], it is thus not difficult to understand that the fatigue data obtained at the lower stress amplitudes would exhibit a larger scatter than the tensile data due to the large microstructural change across the weld and the presence of weld concavity (Figs. 2 and 3).

The S–N plot in Fig. 9 could be expressed using the Basquin equation [30,32],

$$\sigma_a = \sigma'_f (2N_f)^b, \quad (1)$$

Table 2
Tensile properties and fatigue parameters σ_f' and b for HSLA BM, DP980 BM, similar HSLA–HSLA and DP980–DP980 welded joints, and dissimilar HSLA–DP980 welded joints.

Welding type	Yield strength (MPa)	Ultimate tensile strength (MPa)	Elongation (%)	Joint efficiency (%)	Fatigue limit (MPa)	Fatigue ratio	σ_f' (MPa)	b	
HSLA–HSLA	446	529	22.3	97	125	0.236	328	−0.041	Present
HSLA–DP980	467	548	15.4	~100	175	0.319	371	−0.055	study
HSLA BM	455	546	24.7	–	200	0.366	302	−0.023	Ref. [13]
DP980 BM	720	1095	14.2	–	250	0.228	1019	−0.098	
DP980–DP980	720	1067	5.3	97	150	0.141	1169	−0.132	

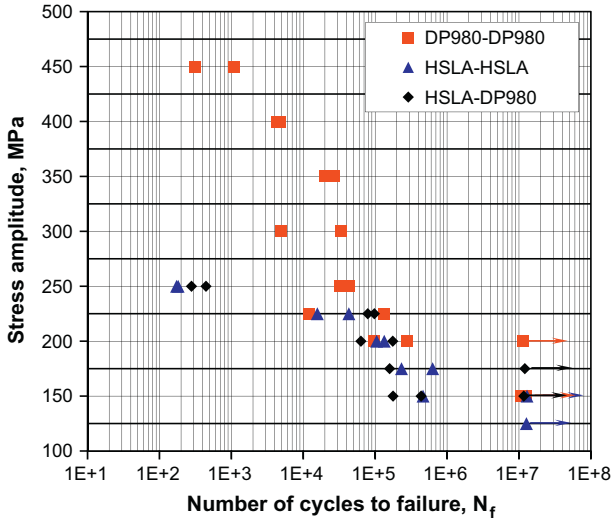

Fig. 9. Comparison of the S–N curves of the HSLA, DP980, and dissimilar welded joints tested at $R = 0.1$, 50 Hz, and room temperature, where the DP980–DP980 and HSLA–HSLA curves are taken from [13].

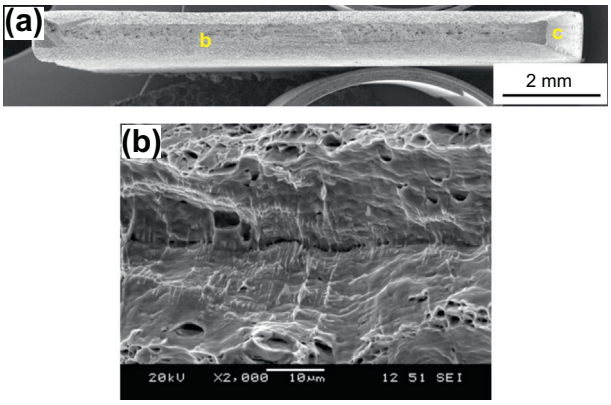

Fig. 11. SEM images illustrating the fatigue fracture surface of a dissimilar HSLA–DP980 welded joint tested at a stress amplitude of 250 MPa: (a) overall view and (b) crack propagation region, where "c" in (a) indicates the necking region.

where σ_a is the cyclic stress amplitude, σ_f' is the fatigue strength coefficient defined by the stress intercept at $2N_f = 1$, N_f is the number of cycles to failure ($2N_f$ is the number of reversals to failure), and b is the fatigue strength exponent. The values of these parameters obtained by fitting the data points according to Eq. (1) are tabulated in Table 2. The fatigue life of the welded joints could be estimated based on the values of σ_f' and b. Eq. (1) indicates that the higher the value of σ_f' and the smaller the absolute value of b, which is always negative, the longer the fatigue life. It is seen from Table 2 that the HSLA-related specimens (i.e., HSLA BM, similar HSLA–HSLA welded joints, and dissimilar HSLA–DP980 welded joints) had an equivalent set of σ_f' and b values within the experimental scatter, giving rise to roughly the same overall fatigue life (Fig. 9). In comparison with the HSLA-related specimens, while the absolute value of fatigue strength exponent, $|b|$, of the DP980 BM and similar DP980–DP980 welded joints was higher, which was supposed to give rise to a lower fatigue life, the fatigue strength coefficient σ_f' was nearly or over three times higher, leading to a much higher fatigue life. Such a seemingly conflicting set of σ_f' and b values via their combined effects determine the overall fatigue of these similar and dissimilar welded joints and BM. It should be noted that the lower fatigue ratio (i.e., the ratio of the fatigue limit to the UTS) in the DP980 BM and similar DP980–DP980 welded joints, in comparison with to the HSLA-related specimens, was mainly due to the fact that the UTS of the DP980–DP980 welded joints had nearly twice that of the HSLA and only had a slightly higher fatigue limit (Table 2). These conclusions were also reported by Xu et al. [13] using similar HSLA–HSLA and DP980–DP980 welded joints.

3.5. Fractography

Some typical SEM images of a fatigue fracture surface of a dissimilar HSLA–DP980 welded joint tested at a high stress amplitude of 250 MPa are shown in Fig. 11. Interestingly, no clear crack initiation area could be seen (Fig. 11a) as the failure was primarily

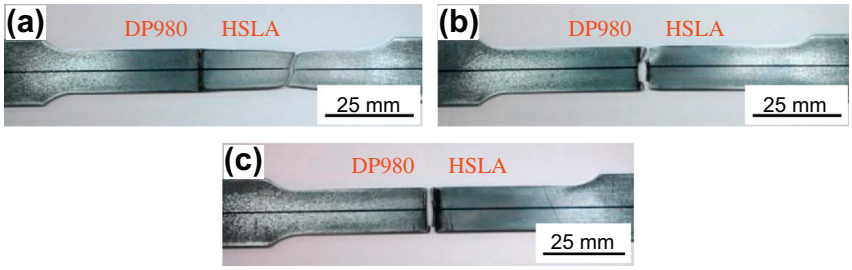

Fig. 10. Typical fatigue failure locations in the dissimilar HSLA–DP980 welded joints at stress amplitudes of (a) 250 MPa, (b) 200 MPa, and (c) 175 MPa.

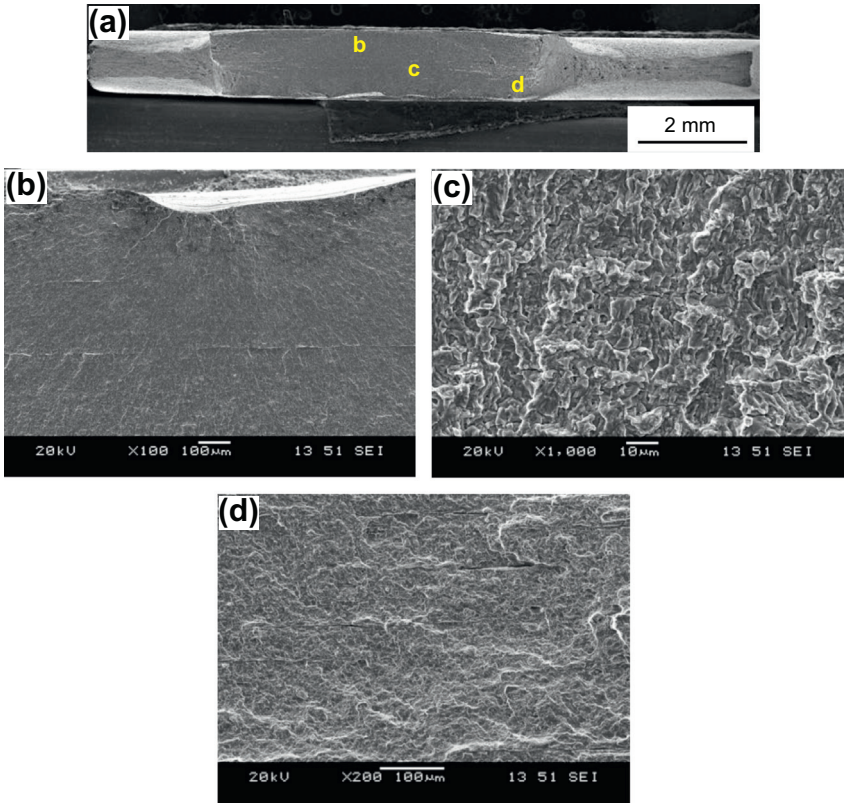

Fig. 12. SEM micrographs depicting the fatigue fracture surface in a dissimilar HSLA–DP980 welded joint tested at a stress amplitude of 200 MPa: (a) overall view, (b) fatigue crack initiation region, (c) crack propagation region, and (d) final fast fracture interface.

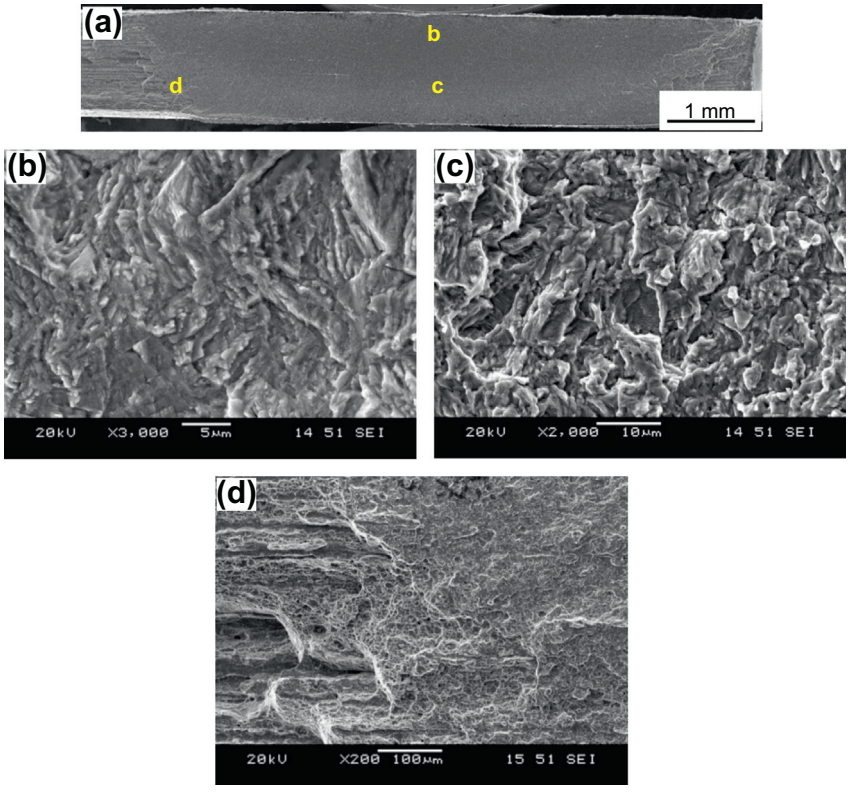

Fig. 13. SEM micrographs of the fatigue fracture surface in a dissimilar HSLA–DP980 welded joint tested at a stress amplitude of 150 MPa: (a) overall view, (b) fatigue crack initiation region, (c) crack propagation region, and (d) final fast fracture interface.

caused by the yielding in the BM region on the HSLA side (Fig. 10a) due to the high maximum stress beyond the YS of HSLA at this cyclic stress level, which could be confirmed by the tapered region seen around the fracture surface, indicated by "c" in Fig. 11a. Fatigue crack propagation was basically characterized by the occurrence of fatigue striations in conjunction with the dimples and plastic ridges, as shown in Fig. 11b [13].

Figs. 12 and 13 show typical fracture surfaces of the dissimilar HSLA–DP980 welded joints that failed at stress amplitudes of 200 MPa and 150 MPa, respectively. Since the failure occurred in the weld area in this case at the intermediate and lower stress amplitudes (Fig. 10b and c), rather than causing by the plastic deformation at the high stress amplitude of 250 MPa (Figs. 10a and 11), fatigue crack initiation site can be clearly identified, as marked as "b" in the overall images of Figs. 12a and 13a. From the magnified images showing the crack initiation area in Figs. 12b and 13b, it is seen that crack initiation basically occurred from the specimen surface due to the stress concentration arising from the presence of concavity. Fatigue striations can be seen in the propagation region in Figs. 12c and 13c, where fatigue damage progressively accumulated as the propagation approached the final fracture, with the border area of the transition from the fatigue crack propagation to the final fast fracture shown in Figs. 12d and 13d. The final fast fracture area consisted of characteristic dimples [13]. This is understandable since HSLA is very ductile with a ductility of ~25% (Table 2). It should be noted that, while in the dissimilar HSLA–DP980 welded joints a soft zone was present on the DP980 side and no soft zone was present at all on the HSLA side (Figs. 6 and 7), fatigue failure at the lower stress amplitudes still occurred close to the HSLA due to the lower hardness or strength of HSLA itself. Furthermore, all tensile test samples were observed to fail in the BM on the HSLA side, like the situation shown in Figs. 10a and 11a. Therefore, it can be concluded from the present study that the existence of a soft zone in the dissimilar HSLA–DP980 welded joints, as long as it is small and narrow, would not affect both the tensile properties and fatigue resistance. To enhance the fatigue strength of such dissimilar welded joints further efforts are needed to get rid of the weld concavity.

4. Conclusions

Based on the present study on the microstructure, hardness profile, tensile properties, and fatigue performance of HSLA–DP980 dissimilar welded joints, the following conclusions can be drawn:

(1) The fiber laser welded dissimilar HSLA–DP980 joints consisted of a microstructure lying in-between those of similar HSLA–HSLA and DP980–DP980 welded joints. Due to the fast cooling during FLW, the narrow FZ was composed of a highly martensitic structure. The HAZ on the DP980 side of the weld contained some newly formed martensite and partially tempered martensite.

(2) A characteristic asymmetric hardness profile across the dissimilar HSLA–DP980 welded joint with a higher hardness on the DP980 side and a lower hardness on the HSLA side was observed. While a soft zone appeared on the DP980 side, it was absent on the HSLA side. Inside the FZ two distinct hardness sub-regions (i.e., ~390HV on the HSLA side and ~410HV on the DP980 side) were observed due to the difference in the carbon and manganese contents between HSLA and DP980 along with the fast cooling during FLW.

(3) The presence of soft zone on the DP980 side of the dissimilar welded joints was observed to have no effect on the tensile properties, since the lowest hardness value at the valley of soft zone (255HV) was still higher than that of the HSLA BM (167HV). A joint efficiency of 97–100% was achieved with respect to the HSLA. While the strain to failure was lower in the similar DP980–DP980 welded joints, it had a remarkable (~threefold) increase in the dissimilar HSLA–DP980 welded joints.

(4) While the fatigue strength of the dissimilar HSLA–DP980 welded joints was lower than that of similar DP980–DP980 welded joints, it was equivalent to the similar HSLA–HSLA welded joints.

(5) Failure occurred in the BM on the HSLA side in the tensile tests as well as in the fatigue tests at high cyclic stress levels, where yielding was a dominant form of failure. At the intermediate and lower cyclic stress levels, fatigue failure occurred in the weld area due to the higher degree of sensitivity to the weld concavity.

(6) Fatigue crack initiation basically occurred from the specimen surface due to the stress concentration arising from the presence of concavity.

Acknowledgements

The authors would like to thank the Natural Sciences and Engineering Research Council of Canada (NSERC) and AUTO21 Network of Centers of Excellence for providing financial support. The financial support from International Zinc Association (IZA) and ArcelorMittal Dofasco is highly acknowledged. One of the authors (D.L. Chen) is grateful for the financial support by the Premier's Research Excellence Award (PREA), NSERC-Discovery Accelerator Supplement (DAS) Award, Canada Foundation for Innovation (CFI), and Ryerson Research Chair (RRC) program. The authors would like to thank Dr. J. Chen and Dr. Y.L. He (CANMET-Materials Technology Laboratory, Natural Resources Canada, Hamilton, Canada), Mr. E. Biro (ArcelorMittal Global Research, Hamilton, Canada), and Dr. J. Villafuerte (CenterLine (Windsor) Ltd., Windsor, Canada) for their support and helpful discussion. The assistance of Q. Li, A. Machin, J. Amankrah, and R. Churaman in performing the experiments is gratefully acknowledged.

References

[1] Murray J, King D. Oil's tipping point has passed. Nature 2012;481:433–5.
[2] Joost WJ. Reducing vehicle weight and improving US energy efficiency – using integrated computational materials engineering. JOM 2012;64:1032–8.
[3] Kim HJ, Keoleian GA, Skerlos SJ. Economic assessment of greenhouse gas emissions reduction by vehicle light weighting using aluminum and high-strength steel. J Ind Eco 2011;15:64–80.
[4] Li HZ, Sun GY, Li GY, Gong ZH, Liu DH, Li Q. On twist springback in advanced high-strength steels. Mater Des 2011;32:3272–9.
[5] Tang L, Wang H, Li GY. Advanced high strength steel springback optimization by projection-based heuristic global search algorithm. Mater Des 2013;43:426–37.
[6] Wang WR, He CW, Zhao ZH, Wei XC. The limit drawing ratio and formability prediction of advanced high strength dual-phase steels. Mater Des 2011;32:3320–7.
[7] Khan MS, Bhole SD, Chen DL, Boudreau G, Biro E, Van Deventer J. Resistance spot welding characteristics and mechanical properties of galvannealed HSLA 350 steel. Can Metall Quart 2009;48:303–10.
[8] Anand D, Chen DL, Bhole SD, Andreychuk P, Boudreau G. Fatigue behavior of tailor (laser) welded blanks for automotive applications. Mater Sci Eng A 2006;420(1–2):199–207.
[9] Panda SK, Li J, Baltazar Hernandez VH, Zhou Y, Goodwin F. Effect of weld location, orientation, and strain path on forming behavior of AHSS tailor welded blanks. J Eng Mater Technol 2010;132:041003-1–041003-11.
[10] Khan MS, Bhole SD, Chen DL, Boudreau G, Biro E, van Deventer J. Welding behavior, microstructure and mechanical properties of dissimilar resistance spot welds between galvannealed HSLA350 and DP600 steels. Sci Technol Weld Join 2009;14:616–25.
[11] Ma C, Chen DL, Bhole SD, Boudreau G, Lee A, Biro E. Microstructure and fracture characteristics of spot-welded DP600 steel. Mater Sci Eng A 2008;485:334–46.

[12] Patel VK, Bhole SD, Chen DL. Formation of zinc interlayer texture during dissimilar ultrasonic spot welding of magnesium and high strength low alloy steel. Mater Des 2013;45:236–40.
[13] Xu W, Westerbaan D, Nayak SS, Chen DL, Goodwin F, Zhou Y. Tensile and fatigue properties of fiber laser welded high strength low alloy and DP980 dual-phase steel joints. Mater Des 2013;43:373–83.
[14] Kwon O, Baik SC. Manufacture and application of advanced high strength steel sheets for auto manufacture, Pohang 2005: POSCO; 785–90.
[15] Farabi N, Chen DL, Zhou Y. Tensile properties and work hardening behavior of laser-welded dual-phase steel joints. J Mater Eng Perform 2012;21:222–30.
[16] Xia M, Sreenivasan N, Lawson S, Zhou Y, Tian Z. A comparative study of formability of diode laser welds in DP980 and HSLA steels. J Eng Mater Technol 2007;129:446–52.
[17] Farabi N, Chen DL, Li J, Zhou Y, Dong SJ. Microstructure and mechanical properties of laser welded DP600 steel joints. Mater Sci Eng A 2010;527:1215–22.
[18] Cao J, Gong Y, Zhu K, Yang ZG, Luo XM, Gu FM. Microstructure and mechanical properties of dissimilar materials joints between T92 martensitic and S304H austenitic steels. Mater Des 2011;32:2763–70.
[19] Farabi N, Chen DL, Zhou Y. Microstructure and mechanical properties of laser welded dissimilar DP600/DP980 dual-phase steel joints. J Alloys Compd 2011;509:982–9.
[20] Quinto L, Costa A, Miranda R, Yapp D, Kumar V, Kong CJ. Welding with high power fiber lasers – a preliminary study. Mater Des 2007;28:1231–7.
[21] Cui CY, Cui XG, Ren XD, Liu TT, Hu JD, Wang YM. Microstructure and microhardness of fiber laser butt welded joint of stainless steel plates. Mater Des 2013;49:761–4.
[22] Chen HC, Pinkerton AJ, Li L, Liu Z, Mistry AT. Gap-free fibre laser welding of Zn-coated steel on Al alloy for light-weight automotive applications. Mater Des 2011;32:495–504.
[23] Sokolova M, Salminena A, Kuznetsovb M, Tsibulskiyb I. Laser welding and weld hardness analysis of thick section S355 structural steel. Mater Des 2011;32:5127–31.
[24] Hazratinezhad M, Mostafa Arab NB, Sufizadeh AR, Torkamany MJ. Mechanical and metallurgical properties of pulsed neodymium-doped yttrium aluminum garnet laser welding of dual phase steels. Mater Des 2012;33:83–7.
[25] Kou S. Welding metallurgy. 2nd ed. Hoboken (NJ): John Wiley & Sons Inc; 2003.
[26] Porter DA, Easterling KE. Phase transformations in metals and alloys. 2nd ed. Boca Ratton (FL): Taylor & Francis Group; 1992.
[27] Song Y, Hua L, Chu D, Lan J. Characterization of the inhomogeneous constitutive properties of laser welding beams by the micro-Vickers hardness test and the rule of mixture. Mater Des 2012;37:19–27.
[28] Xu W, Westerbaan D, Nayak SS, Chen DL, Goodwin F, Biro E, et al. Microstructure and fatigue performance of single and multiple linear fiber laser welded DP980 dual-phase steel. Mater Sci Eng A 2012;553:51–7.
[29] Alam MM, Karlsson J, Kaplan AFH. Generalising fatigue stress analysis of different laser weld geometries. Mater Des 2011;32:1814–23.
[30] Dieter GE. Mechanical metallurgy. 3rd ed. New York: McGraw-Hill; 1986.
[31] Chapetti MD, Katsura N, Tagawa T, Miyata T. Static strengthening and fatigue blunt-notch sensitivity in low-carbon steels. Int J Fatigue 2001;23:207–14.
[32] Farabi N, Chen DL, Zhou Y. Fatigue properties of laser welded dual-phase steel joints. Procedia Eng 2010;2:835–43.